ACS Catalysis

pubs.acs.org/acscatalysis
Research Article

Essential Insight of Direct Electron Transfer-Type Bioelectrocatalysis by Membrane-Bound D-Fructose Dehydrogenase with Structural Bioelectrochemistry

Yohei Suzuki, Fumiaki Makino, Tomoko Miyata, Hideaki Tanaka, Keiichi Namba, Kenji Kano, Keisei Sowa,* Yuki Kitazumi, and Osamu Shirai

Cite This: *ACS Catal.* 2023, 13, 13828−13837

ABSTRACT: Flavin adenine dinucleotide-dependent D-fructose dehydrogenase (FDH) from *Gluconobacter japonicus* NBRC3260, a membrane-bound heterotrimeric flavohemoprotein capable of direct electron transfer (DET)-type bioelectrocatalysis, was investigated from the perspective of structural biology, bioelectrochemistry, and protein engineering. DET-type reactions offer several benefits in biomimetics (e.g., biofuel cells, bioreactors, and biosensors) owing to their mediator-less configuration. FDH provides an intense DET-type catalytic signal; therefore, extensive research has been conducted on the fundamental principles and applications of biosensors. Structural analysis using cryo-electron microscopy and single-particle analysis has revealed the entire FDH structures with resolutions of 2.5 and 2.7 Å for the reduced and oxidized forms, respectively. The electron transfer (ET) pathway during the catalytic oxidation of D-fructose was investigated by using both thermodynamic and kinetic approaches. Structural analysis has shown the localization of the electrostatic surface charges around heme 2*c* in subunit II, and experiments using functionalized electrodes with a controlled surface charge support the notion that heme 2*c* is the electrode-active site. Furthermore, two aromatic amino acid residues (Trp427 and Phe489) were located in a possible long-range ET pathway between heme 2*c* and the electrode. Two variants (W427A and F489A) were obtained by site-directed mutagenesis, and their effects on DET-type activity were elucidated. The results have shown that Trp427 plays an essential role in accelerating long-range ET and triples the standard rate constant of heterogeneous ET according to bioelectrochemical analysis.

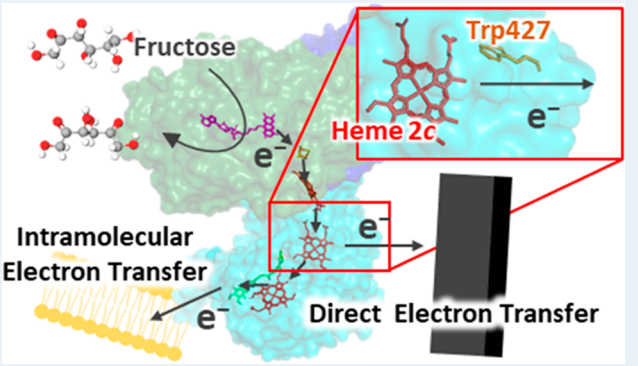

KEYWORDS: *bioelectrocatalysis, direct electron transfer, cryo-electron microscopy, membrane-bound D-fructose dehydrogenase, intramolecular electron transfer*

INTRODUCTION

Oxidoreductases are enzymes that catalyze redox reactions in living organisms. They facilitate biological electron transfer (ET) and play essential roles in several biochemical events (e.g., photosynthesis, respiration, and nitrogen fixation). The variety of these enzymes is extensive, accounting for one-fourth of all enzymes. In contrast, oxidoreductases have been utilized in bioelectrocatalysts to realize a variety of biotechnologies, such as biosensors, biofuel cells, solar fuel production, carbon dioxide capture and utilization, and cofactor-regeneration systems. These systems are based on bioelectrocatalysis, which couples electrode and enzymatic reactions.[1−11]

Several metalloenzymes can communicate electronically with suitable electrodes without redox mediators to shuttle electrons between the enzyme and electrode. This phenomenon has been termed "direct electron transfer (DET)-type bioelectrocatalysis".[12−25] Owing to the mediator-less configuration, the reaction can offer the following benefits in future bioelectrochemical technologies: (i) minimized overvoltage, (ii) low cost, (iii) simple design, (iv) high degree of design freedom, and (v) nontoxic and environmentally friendly properties.[12−25] The third-generation biosensors, which employ a principle of DET-type bioelectrocatalysis to detect the target substances, have been considered ideal and elegant.[26] They are helpful for health management (e.g., self-monitoring of blood glucose (SMBG) or sweat sensing).[27−29] In many cases, DET-type enzymes have a catalytic site that

Received: August 11, 2023
Revised: September 17, 2023
Published: October 12, 2023

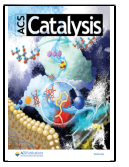

https://doi.org/10.1021/acscatal.3c03769
ACS Catal. 2023, 13, 13828−13837

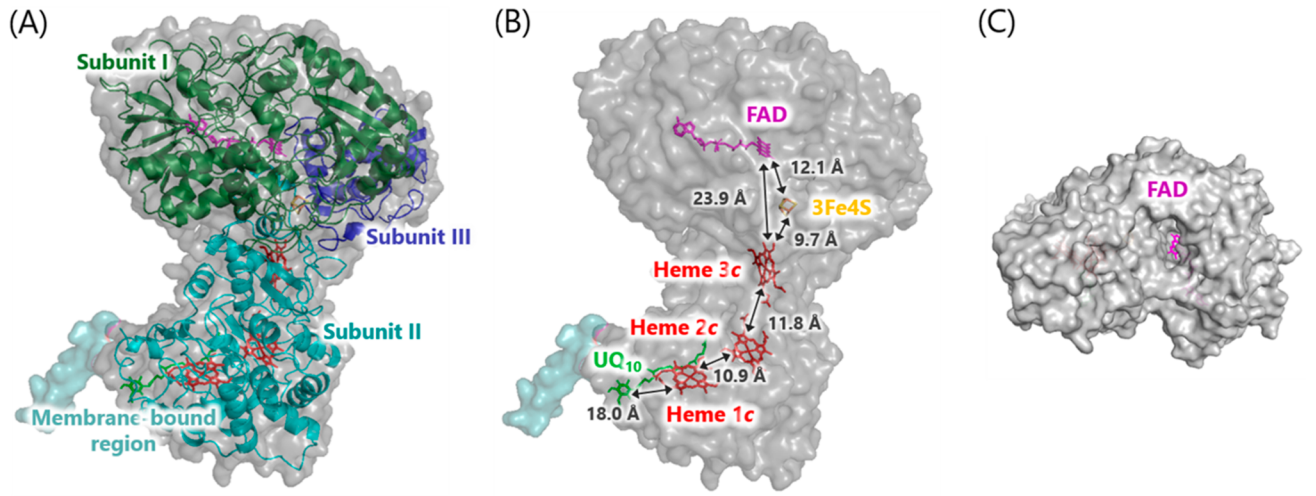

Figure 1. (A) Side view of the entire structure of FDH analyzed by cryo-EM (PDB ID: 8JEJ). The membrane-bound region is shown as a surface model (pale blue) with a superposition of structures in another class of FDH (PDB ID: 7W2J). (B) Geometrical arrangement of cofactors in a heterotrimer. FAD, 3Fe4S, hemes *c*, and UQ_{10} are colored magenta, yellow, red, and green, respectively. Bidirectional arrows show edge-to-edge distances between cofactors. (C) Top view of the entire structure of FDH showing the substrate binding pocket.

catalyzes the redox reaction of the target substrate and an electrode-active site that communicates with an electrode. Metal cofactors (Ni, Fe, W, and Mo) and non-metallocofactors (such as flavin adenine dinucleotide (FAD) and pyrroloquinoline quinone (PQQ)) are known as catalytic sites, whereas heme moieties, iron−sulfur clusters, and other metal centers are generally known as electrode-active sites.[21,30,31]

Membrane-bound quinohemoproteins, flavohemoproteins, and metallohemoproteins have been actively studied as DET-type enzymes for the following reasons: (a) generation of clear catalytic signals, (b) potential as biosensors for organic substrates (such as sugars, alcohols, or aldehydes), (c) variety of mutants, and (d) no loss of cofactors through covalent bonding with an enzyme (in the case of flavohemoproteins and metallohemoproteins).[32] PQQ-dependent alcohol dehydrogenase (ADH)[33] and molybdopterin-containing (Moco) aldehyde dehydrogenase (AlDH)[34] from *Gluconobacter oxydans*, PQQ-dependent ADH and AlDH from *Gluconobacter* sp.33,[35] FAD-dependent glucose dehydrogenase (*Bc*GDH) from *Burkholderia cepacia*,[36] and FAD-dependent D-fructose dehydrogenase (FDH) from *G. japonicus* NBRC 3260[37] are known as DET-type enzymes. They have a heterotrimeric structure with a large subunit that catalyzes substrate oxidation. The subunit containing three heme *c* moieties has a membrane anchor and is physiologically responsible for ET from the substrate to ubiquinone (UQ).[38,39] In addition, the small subunit plays a role in its expression.[40]

We discuss flavohemoproteins in more detail. *Bc*GDH has been investigated for SMBG, and its mechanism and stability have been studied.[38] In addition, a partial three-dimensional (3D) structure of *Bc*GDH, composed of large and small subunits (*Bc*GDH$\gamma\alpha$), was elucidated (PDB ID: 6A2U).[41] The site-directed mutagenesis and electron paramagnetic resonance (EPR) spectrum has indicated that three Cys residues in the Cys-rich region in the large subunit constitute the 3Fe-4S cluster (3Fe4S), which is thought to mediate the ET between FAD and heme *c* moieties.[42] Another partial 3D structure composed of large and small subunits and a truncated cytochrome subunit, leaving only one heme *c* moiety (*Bc*GDH$\gamma\alpha$-trβ), was also elucidated (PDB ID: 8HDD) to support this discussion.[43] However, the overall structure of the membrane-bound subunit, including heme *c* moieties responsible for the electrode-active site, remains unknown. FDH is a particular enzyme with intense DET-type bioelectrocatalytic activity and has been extensively investigated from electrochemistry, protein engineering, and spectroscopy perspectives.[39] FDH comprises subunits I (67 kDa), II (51 kDa), and III (20 kDa). Subunit I contains a covalently bound FAD, and subunit II carries three heme *c* moieties from its N-terminus called hemes 1*c*, 2*c*, and 3*c*.[44,45] The redox potentials of hemes *c* in FDH and several variants were investigated using bioelectrochemical and spectroscopic methods.[46−48] The ET pathway of DET-type bioelectrocatalysis of FDH was examined with site-directed mutagenesis to replace the axial ligand of heme *c* and to delete the heme *c* moiety.[48−50] These studies have shown that the electron is transferred from the reduced FAD through heme 3*c* to heme 2*c* and then to the electrode; heme 1*c* does not seem to be involved in the reaction.[48−50] However, the entire 3D structure of FDH, as well as other membrane-bound quinohemoproteins, flavohemoproteins, and metallohemoproteins, remained unknown until our first discovery of the FDH structure reported in a preprint article in 2022.[51] Therefore, a quantitative discussion of their DET-type reaction was difficult.

In the present study, we aimed to elucidate the 3D structure of FDH using cryo-electron microscopy (cryo-EM) and single-particle image analysis. The ET pathway of the DET-type FDH reaction has been quantitatively discussed from the viewpoints of structural biology, bioelectrochemistry, and protein engineering. Structural analysis has shown the localization of electrostatic surface charges around heme 2*c*, and experiments using functionalized electrodes with a controlled surface charge have supported the idea that heme 2*c* is the electrode-active site. Focusing on aromatic residues that have been reported to enhance long-range ET,[52−57] we constructed variants in which the corresponding residues were each replaced with alanine. Based on the entire structure and the experimental results, we elucidated the enhancement of long-range ET by Trp427, which is located in the middle of the ET pathway from heme 2*c* to the electrode.

https://doi.org/10.1021/acscatal.3c03769
ACS Catal. 2023, 13, 13828−13837

RESULTS AND DISCUSSION

Cryo-EM Structures of FDH. Figure 1A shows the 3D structure of recombinant (native) FDH (rFDH) based on cryo-EM single-particle image analysis with a resolution of 2.5 Å (rFDH-R), which was retained in the reduced form with sodium dithionite. The structure of the FDH oxidized with potassium ferricyanide was also determined with a resolution of 2.7 Å (rFDH-O), and Figure S2 shows the superposition of their 3D structures. Because the root-mean-square deviation value is sufficiently small (0.19 Å), we concluded that the heterotrimeric structure and geometrical arrangement of cofactors in the enzyme were almost identical regardless of the redox equilibrium state. Although rFDH forms a dimer of heterotrimers in solution according to our previous study,[58] the cryo-EM maps after CTF refinement and 3D refinement with C1 symmetry covered the monomer of the heterotrimer that lacks the membrane-bound region at the C-terminus of subunit II (Figures S3 and S4). This is probably due to the structural flexibility of its membrane-bound regions, as inferred from the 3D variability analysis (Figure S5). We previously reported the first entire structure as a dimer of FDH (rFDH-D; Figure S6) in a preprint article in 2022.[51] The resolution of the map, in which two heterotrimers form a dimer through interaction with the membrane-bound regions solubilized by a surfactant (Triton X-100), was much lower (3.6 Å) than those in the present study due to a flexible dimer arrangement (Figure S7).

Figure 1B shows the edge-to-edge distances between the cofactors of rFDH-R. Three of the four sequential cysteine residues in subunit I (Cys885, Cys891, and Cys895) form the 3Fe-4S iron−sulfur cluster (3Fe4S) as in the case of *Bc*GDH[41,42] (Figure S8A and B). Considering the reported limit of 14−20 Å for the long-range ET distance,[59,60] 3Fe4S serves as an ET relay between FAD and heme 3*c*. In addition, clear elongated densities were observed between heme 1*c* and the membrane-bound region in the 3D maps of both rFDH-R and rFDH-O (Figure S8C and D). Based on the physiological role of FDH, we considered that UQ_{10} was the most probable candidate for these densities.[61,62] Reverse-phase high-performance liquid chromatography (HPLC) was performed on the organic extracts of the rFDH solutions, and the results confirmed the presence of UQ_{10} (Figure S9). UQ_{10} was quantified as 1% of the molar amount of rFDH, indicating that UQ_{10} bound weakly and partially to the enzymes. This is consistent with the relatively low resolution of the densities, and similar results have been confirmed in the case of ADH and AlDH from *G. oxydans*.[63] Furthermore, we confirmed a clear cavity around the FAD catalytic site in the top view of the structure (Figure 1C).

Various structural prediction techniques have been developed. For FDH, prediction using SWISS-MODEL (homology prediction tool) was conducted, and possible ET pathways were discussed.[64] AlphaFold2 is also a powerful predictive tool.[65] We compared the results of these prediction techniques with those of our structural analysis. Although the accuracy for subunits I and III was relatively good, the accuracy for subunit II and the heterotrimer was poor (Figures S10 and S11). These results indicate that the prediction accuracy of membrane-bound proteins remains insufficient and the present study provides essential findings in structural biology.

We now discuss the intramolecular ET in rFDH. The long-range ET rate constant (k_{ET}) can be expressed using eq 1, based on Marcus' theory.[66]

$$k_{ET} k^{\circ} \exp\left(\frac{-\lambda}{4RT} + \frac{nF\Delta E}{2RT}\right)\exp(-\beta \Delta d) \quad (1)$$

Here k° is the standard rate constant, λ is the reorganization energy, R is the gas constant, T is the absolute temperature, n is the electron number, F is the Faraday constant, $\Delta E^{\circ\prime}$ is the potential difference between the cofactors, β is the decay coefficient of the long-range ET (assumed to be 1.4 $Å^{-1}$ for proteins in general), and Δd is the edge-to-edge distance between the cofactors. Based on the assumptions reported thus far,[66] eq 1 can be simplified to eq 2.

$$k_{ET} \frac{\left\{k_{ii} k_{jj} f \exp\left(\frac{nF\Delta E}{RT}\right)\right\}^{1/2}}{SK_A} \exp(-\beta \Delta d) \quad (2)$$

Here k_{ii} and k_{jj} are the self-exchange rate constants for the electron donor and acceptor (designated as i and j, respectively), S is the steric factor (≅0.1), and K_A is the encounter equilibrium constant (≅0.4 M^{-1}).[66] The f value in eq 2 is described in the Supporting Information (eq S1). The redox potentials of FAD and hemes *c* were based on previous studies.[47,67] For 3Fe4S, redox titration using EPR was performed to roughly estimate the redox potential (Figures S12 and S13). Moser et al. analyzed data obtained from many intramolecular ET reactions and found that the k_{ET} correlates well with Δd assuming β = 1.4 $Å^{-1}$.[68] Figure 2 shows the thermodynamic and kinetic diagrams of intramolecular ET. Detailed descriptions of the ET rate constants are provided in the Supporting Information (Table S4). This prediction with a general value of β (1.4 $Å^{-1}$) indicates that the ET process between FAD and 3Fe4S seems to be the rate-determining step. However, smaller β values have also been provided to ET in some proteins (e.g., β = 0.66 $Å^{-1}$ for azurin,[69] β = 0.68 $Å^{-1}$ for ruthenated cytochromes[70]). According to previous studies, aromatic residues accelerate long-range ET.[52−57] Although no aromatic amino acid residues were identified in the ET pathway downstream of 3Fe4S, Trp780 was found in the middle of the ET pathway between FAD and 3Fe4S (Figure S15). Accordingly, we hypothesized that Trp780 plays an

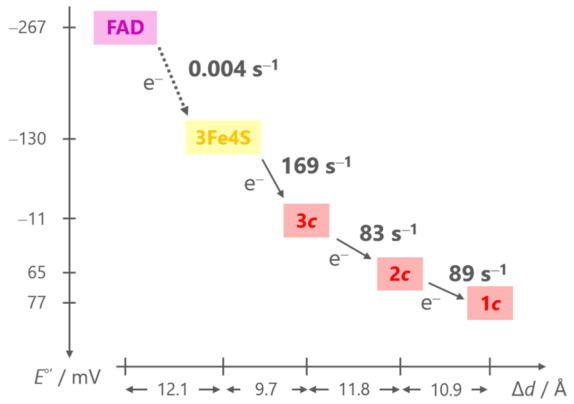

Figure 2. Thermodynamic and kinetic diagram of the intramolecular ET. Horizontal and vertical axes show the edge-to-edge distances between cofactors and their redox potentials, respectively. Arrows represent the ET rate constant predicted by eq 2.

https://doi.org/10.1021/acscatal.3c03769
ACS Catal. 2023, 13, 13828−13837

essential role in the intramolecular ET. To further investigate the hypothesis, the following two studies will be necessary: (1) bioelectrochemical studies of site-directed variants focusing on Trp780 and (2) more accurate quantification of the self-exchange rate constants of the cofactors of FDH.

Bioelectrochemical and Structural Elucidations of DET-Type Bioelectrocatalysis of FDH. Next, we discuss the ET pathway of DET-type bioelectrocatalysis in FDH from bioelectrochemical and structural perspectives. Previous studies have shown that heme 1*c* does not seem to be involved in the reaction and that heme 2*c* is the most likely electrode-active site.[48−50] The distance from the individual cofactors to the α-carbon of the amino acid residues on the enzyme surface indicates that hemes 2*c* and 1*c* are close to the enzyme surface (Figure S16). Furthermore, we attempted to calculate the electrostatic potential distribution on the rFDH surface using the PDB 2PQR web service[71] and PyMOL APBS plugin.[72] Figure 3A and B show the distribution of the surface

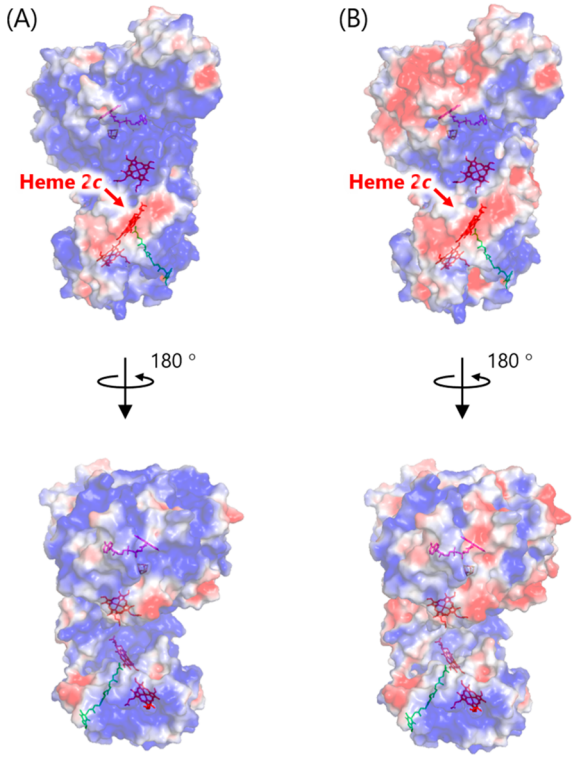

Figure 3. Electrostatic potential distributions of rFDH-R (PDB ID: 8JEJ) at (A) pH 4.5 and (B) pH 6.0 (blue, positive; red, negative) calculated using the PDB 2PQR web service and the PyMOL APBS plugin.

charges at pH 4.5 and 6.0, respectively. Most of the rFDH surface was positively charged at pH 4.5, as inferred from the isoelectric point of rFDH (6.59[73]). Interestingly, the negative charge was concentrated near heme 2*c*. The enzyme surface was less positive at pH 6.0. Based on this unique charge difference around heme 2*c*, we conducted electrochemical measurements using electrodes functionalized with different surface charges.

Glassy carbon (GC) electrodes were modified with multi-walled carbon nanotubes (MWCNTs) for electrochemical measurements. The charging current value at 0.15 V for each electrode ranged between 0.14 and 0.16 mA cm^{-2} (data not shown). Assuming the double-layer capacitance at 0.15 V is identical, we confirmed that the electroactive surface area did not vary significantly between the electrodes. The electrodes were functionalized with 1-pyrene methylamine ($PyNH_2$) or 1-pyrene acetic acid (PyAA)[74] to investigate the differences between the positively and negatively charged electrodes ($PyNH_2$/MWCNT/GCE and PyAA/MWCNT/GCE, respectively). We also investigated the effect of ionic strength on DET-type activity. The enzyme assay in solution indicated that FDH activity remained unchanged with the addition of up to 50 mM NaCl (Figure S17). Thus, 50 mM NaCl was added to the solution to investigate the effects of different ionic strengths on the DET-type reaction. Rotating disk linear sweep voltammograms (RDLSVs) were recorded at pH 4.5 and 6.0 in the presence of 0.2 M D-fructose (Figure S18). At pH 4.5, the DET-type bioelectrocatalytic current density for D-fructose oxidation was higher for $PyNH_2$/MWCNT/GCE than for PyAA/MWCNT/GCE (Figure 4A). In the case of $PyNH_2$/

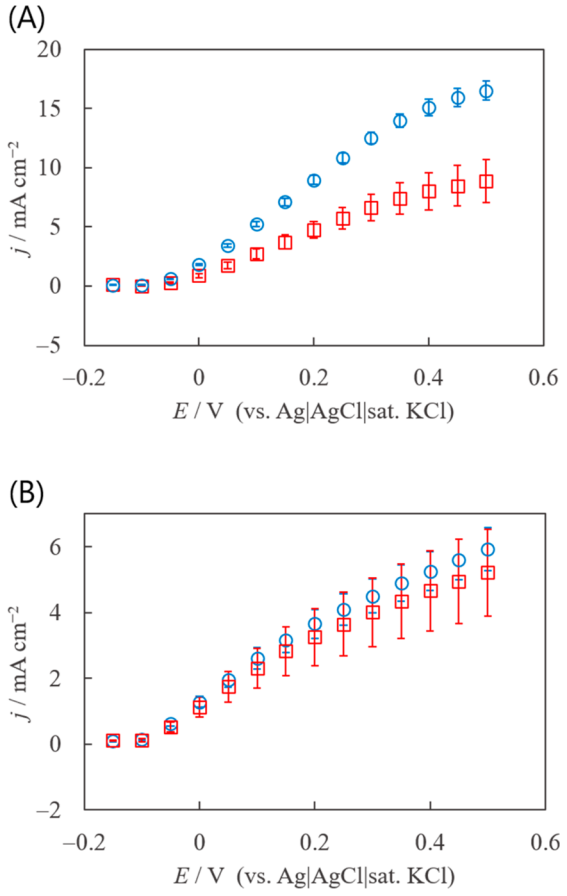

Figure 4. Background-subtracted RDLSVs of D-fructose oxidation at rFDH-adsorbed $PyNH_2$/MWCNT/GCE (blue circles) and PyAA/MWCNT/GCE (red squares) in three-times-diluted McIlvaine buffer containing 0.2 M D-fructose at (A) pH 4.5 or (B) pH 6.0 under Ar-saturated conditions at 25 °C, ω = 4,000 rpm, and ν = 20 mV s^{-1}. Errors were evaluated using the Student's *t*-distribution at a 90% confidence level (N = 5).

MWCNT/GCE, increasing the ionic strength by adding 50 mM NaCl decreased the limiting current density, indicating that the electrostatic attraction was suppressed (Figure S19A). By contrast, in the case of PyAA/MWCNT/GCE, an increase in ionic strength increased the current value, suggesting that the electrostatic repulsion was relaxed (Figure S19A). In

https://doi.org/10.1021/acscatal.3c03769
ACS Catal. 2023, 13, 13828−13837

addition, the current values were almost equal for both electrodes at the high ionic strength of 50 mM NaCl (Figure S19A). Therefore, we concluded that electrostatic interactions between the enzyme and electrode were responsible for the differences in the DET-type reactions. When the electrode surface is positively charged, an attractive electrostatic interaction occurs between the negatively charged region near heme 2*c* and the electrode surface, which induces a favorable orientation of rFDH in the DET-type reaction, with heme 2*c* facing the electrode surface. By contrast, the catalytic current was not significantly affected by the electrode surface charge at pH 6.0 (Figure 4B). This was probably due to an increase in the negative charge on other enzyme surfaces in addition to the region near heme 2*c*. Increasing the ionic strength of the buffer solution did not affect the limiting catalytic current at pH 6.0, either (Figure S19B). These results clearly indicate that heme 2*c* is the electrode-active site in the DET-type reaction of rFDH.

Characterization of Variants Being Focused on Aromatic Residues. In this section, we focus on aromatic amino acid residues that have been reported to enhance ET and discuss the origin of the intense DET-type activity of FDH. Two residues (Trp427 and Phe489) are located in the middle of the ET pathway from heme 2*c* to the top surface (Figure 5), whereas there are no aromatic amino acid residues

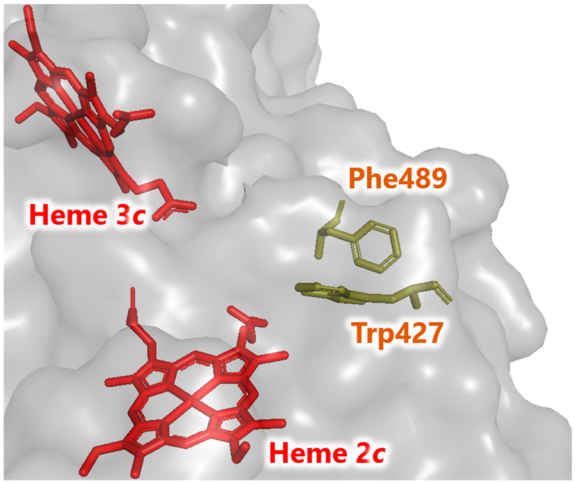

Figure 5. Aromatic residues on the shortest ET pathway from heme 2*c* to the top surface of FDH.

around the other heme *c* moieties. To investigate the possible influence of these residues on the DET-type reaction, we constructed site-directed FDH variants in which either Trp427 or Phe489 was substituted with alanine (F489A or W427A FDH, respectively).

The variants were successfully constructed and purified. These enzymes showed specific activity and an optimal pH similar to those of rFDH (Figure S20). In addition, the oxygen consumption rates (v_{O_2}) of whole cells harboring pSHO13 (for rFDH), pYSF01 (for F489A FDH), or pYSF02 (for W427A FDH) were examined using D-fructose or D-glucose as an electron donor (Figures S21 and S22). No significant differences in v_{O_2} were observed between these variants. Therefore, it can be inferred that no structural changes that would significantly alter the activity occurred in these variants.

We performed electrochemical measurements with these variants using uncharged electrodes to minimize the effects of specific electrostatic interactions. The aryl diazonium salt electro-reduction onto CNT has been widely used as a scaffold to obtain improved performance of DET-type bioelectrocatalysis.[75−77] MWCNT/GCEs modified with 2-aminoanthracene (2-ANT) diazonium were utilized for the measurements to elucidate the effect of aromatic residues.[77] Figure 6A shows

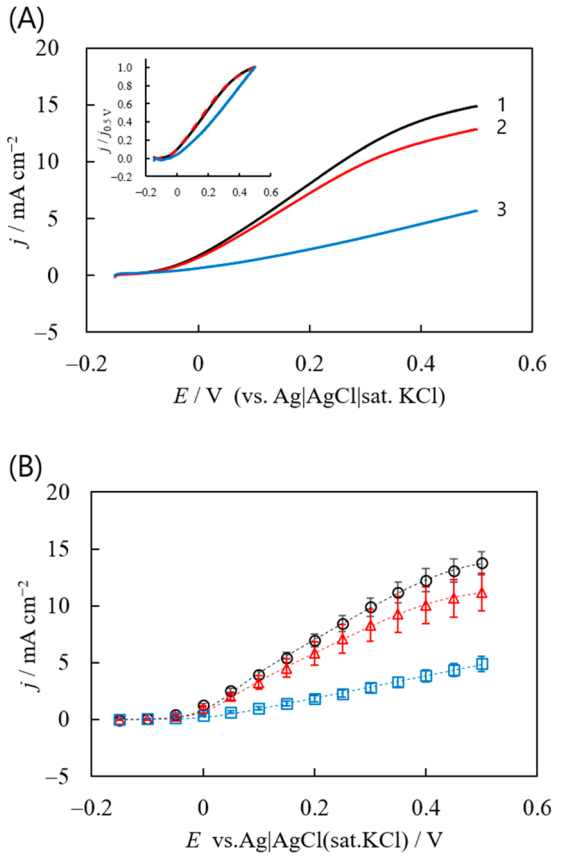

Figure 6. (A) RDLSVs of D-fructose oxidation at the FDH-adsorbed 2-ANT/MWCNT/GCE in three-times-diluted McIlvaine buffer (pH 4.5) containing 0.2 M D-fructose under Ar-saturated conditions at 25 °C, ω = 4,000 rpm, and v = 20 mV s^{-1} (1, rFDH (black); 2, F489A FDH (red); 3, W427A FDH (blue)). The inset shows normalized voltammograms for each catalytic current at 0.5 V. (B) Background-subtracted RDLSVs of D-fructose oxidation at rFDH (black circles), F489A FDH (red triangles), and W427A FDH (blue squares) adsorbed 2-ANT/MWCNT/GCEs. Dashed lines indicate refined curves estimated by non-linear regression analysis based on eq 3. Errors were evaluated using the Student's *t*-distribution at a 90% confidence level (N = 4).

RDLSVs of FDH-adsorbed 2-ANT/MWCNT/GCE recorded in three-times-diluted McIlvaine buffer (pH 4.5) at a rotating speed (ω) of 4000 rpm and a scan rate (v) of 20 mV s^{-1} in the presence of 0.2 M D-fructose. Clear DET-type catalytic waves corresponding to D-fructose oxidation were observed for all of the enzymatic electrodes. The F489A FDH-adsorbed electrode produced a similar catalytic wave approaching a limiting value at 0.5 V, which is nearly identical to rFDH. Therefore, Phe489 did not affect DET-type reactions. By contrast, the W427A FDH-adsorbed electrode showed a linearly increasing part, the so-called residual slope[78] of the steady-state wave. The catalytic current density at 0.5 V was reduced to approximately 35% of

https://doi.org/10.1021/acscatal.3c03769
ACS Catal. 2023, 13, 13828−13837

that of rFDH. This result indicates that Trp427 plays a crucial role in the DET-type reaction of rFDH. Kinetic analyses were performed in the next session to quantitatively evaluate the effect of ET acceleration between heme 2*c* and the electrode surface.

We also constructed two other variants (Δ1*c*-site FDH and W427A Δ1*c*-site FDH) to carefully consider the effect of heme 1*c*. In Δ1*c*-site FDH and W427A Δ1*c*-site FDH, the sequences of heme 1*c* binding site "CAACH", in which two cysteines (Cys235 and Cys238) and a heme 1*c* were covalently linked, were replaced with "AAAAH" to eliminate the heme 1*c* moiety. The v_{O_2} values of the whole cells harboring pYUF23 (for the Δ1*c*-siteFDH) and pYSF03 (for the W427A Δ1*c*-siteFDH) were also examined (Figures S21 and S22). The v_{O_2}values with D-fructose were much lower than those with D-glucose, suggesting that the fructose-oxidizing respiratory chains did not function in the two strains. Considering that the edge-to-edge distance between heme 2*c* and UQ_{10} is too far to transfer electrons (24 Å), these results demonstrated that Δ1*c*-site FDH and W427A Δ1*c*-site FDH did not possess a heme 1*c* moiety. The RDLSVs of the two variant-adsorbed 2-ANT/MWCNT/GCEs are shown in Figure S23. An accelerating effect in the DET-type reaction with Trp427 was also observed in the variants without heme 1*c*. These results support our hypothesis that heme 2*c* is the electrode-active site and that Trp427 plays an essential role in DET.

Bioelectrochemical Discussion on ET Acceleration by a Tryptophan Residue. As reported in previous studies with DET-type enzymes, the DET-type reaction provides the residual slope region on the voltammogram.[12−25] Thus, we estimated the kinetic parameters of the DET-type reaction at the FDH-adsorbed electrodes using a random orientation model.[78,79] In this model, j_{cat} (steady-state catalytic current density of the DET-type reaction) is expressed as follows:[79]

$$j_{cat} = \frac{j_{cat,lim}}{\beta\Delta x(1+\eta)} \ln\left|\frac{\frac{k^{\circ}_{max}}{k_c}(1+\eta)+\eta^{\alpha}}{\frac{k^{\circ}_{max}}{k_c}(1+\eta)\exp(-\beta\Delta x)+\eta^{\alpha}}\right| \quad (3)$$

where $j_{cat,lim}$ is the limiting catalytic current density, k°_{max} is the standard rate constant of the heterogeneous ET at the closest approach in the best orientation of the enzyme, Δx is the difference in the distance between the closest and farthest approaches of the redox center of the electroactive enzyme, k_c is the catalytic constant of the enzyme, and α is the transfer coefficient (0.5, in general).[68] η is defined as follows:

$$\eta = \exp\left\{\frac{n'_E F}{RT}(E^{\circ\prime}_E - E)\right\} \quad (4)$$

where n'_E is the number of electrons in the rate-determining step of the heterogeneous ET (1, in general), E is the electrode potential, and $E^{\circ\prime}_E$ is the formal potential of the electrode-active site. The background-subtracted catalytic currents were used for the analysis. Equation 3 was fitted to the steady-state catalytic waves using non-linear regression analysis in Gnuplot using k°_{max}/k_c, $\beta\Delta x$, and $j_{cat,lim}$ as adjustable parameters by setting α = 0.5. The $E^{\circ\prime}_E$ value was set to 0.032 V based on the non-catalytic signal reported previously.[73]

We successfully analyzed the data for rFDH and F489A FDH with a good fit (Figure 6B). The refined data are summarized in Table 1. The limiting currents of the W427A FDH-adsorbed electrodes could not be determined experimentally, and it was not easy to precisely evaluate the amount of effective enzyme on the electrode. Accordingly, we performed the analysis by fixing either $\beta\Delta x$ or $j_{cat,lim}$, which contributes to the magnitude of the limiting current. We obtained a good fit for W427A FDH in the analysis at $\beta\Delta x \geq$ 20 Å (Figure 6B, Table S5). Although the values of $\beta\Delta x$ and $j_{cat,lim}$ are mutually dependent, the value of k°_{max}/k_c was not affected by $\beta\Delta x$ under the conditions ($\beta\Delta x \geq$ 20 Å). Concerning k°_{max}/k_c, the value for W427A FDH was approximately one-third of those for rFDH and F489A FDH. Because it is reasonable to assume the same k_c for these variants, the acceleration effect of Trp427 is considered to have tripled the value of k°_{max}.

Table 1. Refined Parameters by the Non-linear Regression Analysis of Voltammograms[a]

FDH	k°_{max}/k_c	$\beta\Delta x$	$j_{cat,lim}$/mA cm^{-2}
rFDH	4.6 ± 0.2	9.7 ± 0.1	14 ± 1
F489A FDH	4.2 ± 0.4	9.2 ± 0.3	11 ± 2
W427A FDH	1.5 ± 0.2[b]	27 ± 3[b]	14[b]

[a]Errors were evaluated from Student's *t*-distribution at a 90% confidence level (N = 4). [b]Analytical result assuming $j_{cat,lim}$ = 14 mA cm^{-2}

When we fixed $\beta\Delta x$ = 9.7 based on the analytical result of rFDH, the fitting curve for W427A FDH-adsorbed electrodes showed a sigmoidal character (Figure S24). This characteristic is not consistent with the linear characteristics obtained in the experiments. In addition to k_c, similar effective amounts of adsorbed enzyme can be reasonably assumed for these variants. Thus, the $j_{cat,lim}$ value (5 ± 1 mA cm^{-2}) obtained when fixing $\beta\Delta x$ at 9.7, which is quite smaller than that for rFDH, is also not acceptable (Table S5). Accordingly, this result suggests that $\beta\Delta x$ of W427A FDH is larger than that of rFDH. Because Δx can be assumed to be identical among site-directed variants, the apparent β value in the long-range ET pathway from heme 2*c* to the electrode (approximately 10−14 Å) is also suppressed by Trp427.

Finally, the two different pathways for intramolecular ET and DET of FDH are shown in Scheme 1. In solution, intramolecular ET proceeds in the order from FAD, 3Fe4S, heme 3*c*, heme 2*c*, heme 1*c*, and UQ_{10} to the respiratory chain. By contrast, in the DET-type reaction, the ET route branches off from heme 2*c* and the electrons from the substrates are transferred to FAD, 3Fe4S, heme 3*c*, heme 2*c*, and the electrode in this order.

CONCLUSIONS

In this study, we clarified the 3D structure of FDH using cryo-EM and single-particle image analysis. This is the first study to report the entire structures of membrane-bound flavohemoproteins, quinohemoproteins, and metallohemoproteins capable of DET-type bioelectrocatalysis. Long-range ET kinetics through FAD, 3Fe4S, and hemes 3*c*, 2*c*, and 1*c* were examined based on Marcus' theory. In addition, heme 2*c* is identified as the electrode-active site in the DET-type reaction of FDH from structural biology and bioelectrochemical viewpoints. Furthermore, the ET rate between heme 2*c* and the electrode decreases significantly when Trp427 is substituted with alanine. Kinetic analysis of steady-state catalytic waves has revealed that Trp427 triples the value of k°_{max} in the ET. These findings provide vital information for searching for critical

https://doi.org/10.1021/acscatal.3c03769
ACS Catal. 2023, 13, 13828−13837

Scheme 1. Illustration of the Intramolecular ET and DET Pathways in rFDH, W427A FDH, and F489A FDH

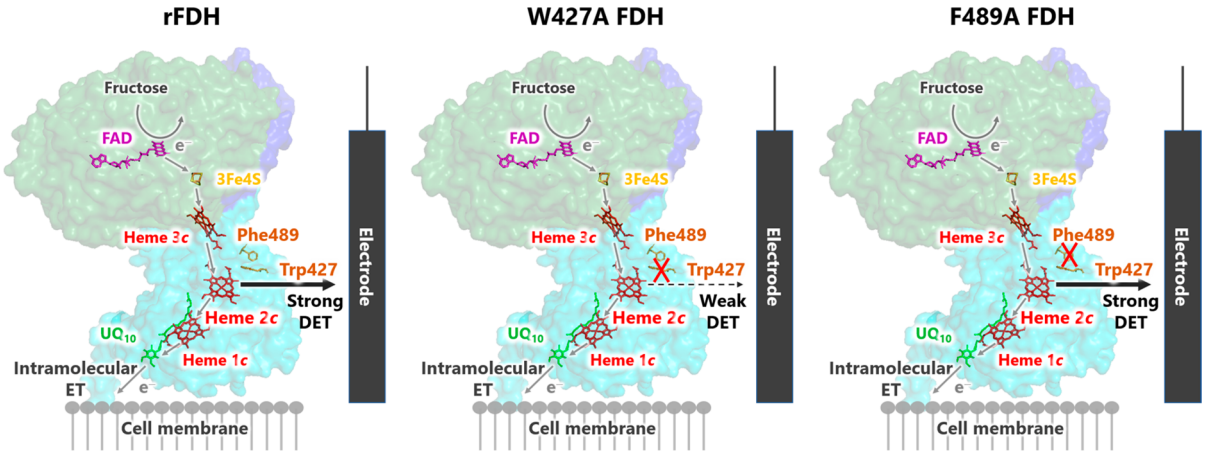

elements for DET-type reactions and a reasonable explanation for the outstanding DET-type activity of FDH. A previous study also reported that the "double-tryptophan" variant, which was constructed by the substitution with Trp, enhanced the intramolecular ET.[52] The appropriate mutation of aromatic residues to accelerate ET between an enzyme and an electrode will be a novel way to create new DET-type enzymes and innovative biomimetics.

■ ASSOCIATED CONTENT

Supporting Information

The Supporting Information is available free of charge at https://pubs.acs.org/doi/10.1021/acscatal.3c03769.

Experimental section, detailed explanations of analytical models, cryo-EM analysis, biochemical assays, structure of rFDH-R, detection of UQ_{10}, EPR analysis, and additional electrochemical data (PDF)

Accession Codes

Cryo-EM structures were deposited in the Protein Data Bank for rFDH-R (PDB ID: 8JEJ), rFDH-O (PDB ID: 8JEK) and rFDH-D (PDB ID: 7W2J and 7WSQ).

■ AUTHOR INFORMATION

Corresponding Author

Keisei Sowa − *Division of Applied Life Sciences, Graduate School of Agriculture, Kyoto University, Sakyo, Kyoto 606-8502, Japan;* orcid.org/0000-0001-9767-4922; Email: sowa.keisei.2u@kyoto-u.ac.jp

Authors

Yohei Suzuki − *Division of Applied Life Sciences, Graduate School of Agriculture, Kyoto University, Sakyo, Kyoto 606-8502, Japan*

Fumiaki Makino − *Graduate School of Frontier Biosciences, Osaka University, Suita, Osaka 565-0871, Japan; JEOL Ltd., Akishima, Tokyo 196-8558, Japan*

Tomoko Miyata − *Graduate School of Frontier Biosciences, Osaka University, Suita, Osaka 565-0871, Japan*

Hideaki Tanaka − *Institute for Protein Research, Osaka University, Suita, Osaka 565-0871, Japan*

Keiichi Namba − *Graduate School of Frontier Biosciences, Osaka University, Suita, Osaka 565-0871, Japan; RIKEN Center for Biosystems Dynamics Research, Suita, Osaka 565-0874, Japan; RIKEN SPring-8 Center, Sayo, Hyogo 679-5198, Japan; JEOL YOKOGUSHI Research Alliance Laboratories, Osaka University, Suita, Osaka 565-0871, Japan*

Kenji Kano − *Center for Advanced Science and Innovation, Kyoto University, Gokasho, Uji, Kyoto 611-0011, Japan;* orcid.org/0000-0002-4667-7020

Yuki Kitazumi − *Division of Applied Life Sciences, Graduate School of Agriculture, Kyoto University, Sakyo, Kyoto 606-8502, Japan*

Osamu Shirai − *Division of Applied Life Sciences, Graduate School of Agriculture, Kyoto University, Sakyo, Kyoto 606-8502, Japan*

Complete contact information is available at: https://pubs.acs.org/10.1021/acscatal.3c03769

Notes

The authors declare no competing financial interest.

■ ACKNOWLEDGMENTS

This research was supported by the Platform Project for Supporting Drug Discovery and Life Science Research (Basis for Supporting Innovative Drug Discovery and Life Science Research (BINDS)) from AMED under Grant JP22ama121003 to K.N., JSPS KAKENHI Grant JP21H01961 to Y.K., JSPS KAKENHI Grant JP22K14831 to K.S., and FY 2022 Kusunoki 125 of Kyoto University 125th Anniversary Fund to K.S. This study was supported in-part by the Program for the Development of Next-generation Leading Scientists with Global Insight (L-INSIGHT), sponsored by the Ministry of Education, Culture, Sports, Science and Technology (MEXT), Japan. We express our gratitude to Mr. Hirou Kaku, Mr. Koryu Ou, and Mr. Yasuyuki Hamano for their financial support. We thank Dr. Hideto Matsuoka of the Graduate School of Science, Osaka City University for his technical assistance with the EPR measurements. We would also like to thank Editage (www.editage.com) for the English language editing.

■ REFERENCES

(1) Willner, I.; Katz, E.; Willner, B. Electrical Contact of Redox Enzyme Layers Associated with Electrodes: Routes to Amperometric Biosensors. *Electroanalysis* **1997**, *9* (13), 965−977.

(2) Habermüller, K.; Mosbach, M.; Schuhmann, W. Electron-Transfer Mechanisms in Amperometric Biosensors. *Fresenius. J. Anal. Chem.* **2000**, *366* (6−7), 560−568.

(3) Barton, S. C.; Gallaway, J.; Atanassov, P. Enzymatic Biofuel Cells for Implantable and Microscale Devices. *Chem. Rev.* **2004**, *104* (10), 4867−4886.
(4) Bartlett, P. N. *Bioelectrochemistry: Fundamentals, Experimental Techniques and Applications*; John Wiley & Sons, 2008. DOI: 10.1002/9780470753842.
(5) Cosnier, S.; Gross, A. J.; Le Goff, A.; Holzinger, M. Recent Advances on Enzymatic Glucose/Oxygen and Hydrogen/Oxygen Biofuel Cells: Achievements and Limitations. *J. Power Sources* **2016**, *325*, 252−263.
(6) Zhao, C. E.; Gai, P.; Song, R.; Chen, Y.; Zhang, J.; Zhu, J. J. Nanostructured Material-Based Biofuel Cells: Recent Advances and Future Prospects. *Chem. Soc. Rev.* **2017**, *46* (5), 1545−1564.
(7) Mano, N.; De Poulpiquet, A. O_2 Reduction in Enzymatic Biofuel Cells. *Chem. Rev.* **2018**, *118* (5), 2392−2468.
(8) Xiao, X.; Xia, H. Q.; Wu, R.; Bai, L.; Yan, L.; Magner, E.; Cosnier, S.; Lojou, E.; Zhu, Z.; Liu, A. Tackling the Challenges of Enzymatic (Bio)Fuel Cells. *Chem. Rev.* **2019**, *119* (16), 9509−9558.
(9) Chen, H.; Simoska, O.; Lim, K.; Grattieri, M.; Yuan, M.; Dong, F.; Lee, Y. S.; Beaver, K.; Weliwatte, S.; Gaffney, E. M.; Minteer, S. D. Fundamentals, Applications, and Future Directions of Bioelectrocatalysis. *Chem. Rev.* **2020**, *120* (23), 12903−12993.
(10) Bollella, P.; Katz, E. Enzyme-Based Biosensors: Tackling Electron Transfer Issues. *Sensors (Switzerland)* **2020**, *20* (12), 3517.
(11) Kano, K.; Shirai, O.; Kitazumi, Y.; Sakai, K.; Xia, H.-Q. *Enzymatic Bioelectrocatalysis*; Springer, 2021. DOI: 10.1007/978-981-15-8960-7
(12) Ghindilis, A. L.; Atanasov, P.; Wilkins, E. Enzyme-Catalyzed Direct Electron Transfer: Fundamentals and Analytical Applications. *Electroanalysis* **1997**, *9* (9), 661−674.
(13) Ferapontova, E. E. Direct Peroxidase Bioelectrocatalysis on a Variety of Electrode Materials. *Electroanalysis* **2004**, *16* (13−14), 1101−1112.
(14) Shleev, S.; Tkac, J.; Christenson, A.; Ruzgas, T.; Yaropolov, A. I.; Whittaker, J. W.; Gorton, L. Direct Electron Transfer between Copper-Containing Proteins and Electrodes. *Biosens. Bioelectron.* **2005**, *20* (12), 2517−2554.
(15) Léger, C.; Bertrand, P. Direct Electrochemistry of Redox Enzymes as a Tool for Mechanistic Studies. *Chem. Rev.* **2008**, *108* (7), 2379−2438.
(16) Falk, M.; Blum, Z.; Shleev, S. Direct Electron Transfer Based Enzymatic Fuel Cells. *Electrochim. Acta* **2012**, *82*, 191−202.
(17) Karyakin, A. A. Principles of Direct (Mediator Free) Bioelectrocatalysis. *Bioelectrochemistry* **2012**, *88*, 70−75.
(18) Sarauli, D.; Xu, C.; Dietzel, B.; Schulz, B.; Lisdat, F. A Multilayered Sulfonated Polyaniline Network with Entrapped Pyrroloquinoline Quinone-Dependent Glucose Dehydrogenase: Tunable Direct Bioelectrocatalysis. *J. Mater. Chem. B* **2014**, *2* (21), 3196−3203.
(19) Milton, R. D.; Minteer, S. D. Direct Enzymatic Bioelectrocatalysis: Differentiating between Myth and Reality. *J. R. Soc. Interface* **2017**, *14* (131), 20170253.
(20) Jenner, L. P.; Butt, J. N. Electrochemistry of Surface-Confined Enzymes: Inspiration, Insight and Opportunity for Sustainable Biotechnology. *Curr. Opin. Electrochem.* **2018**, *8*, 81−88.
(21) Yates, N. D. J.; Fascione, M. A.; Parkin, A. Methodologies for "Wiring" Redox Proteins/Enzymes to Electrode Surfaces. *Chem. - A Eur. J.* **2018**, *24* (47), 12164−12182.
(22) Bollella, P.; Gorton, L.; Antiochia, R. Direct Electron Transfer of Dehydrogenases for Development of 3rd Generation Biosensors and Enzymatic Fuel Cells. *Sensors (Switzerland)* **2018**, *18* (5), 1319.
(23) Evans, R. M.; Siritanaratkul, B.; Megarity, C. F.; Pandey, K.; Esterle, T. F.; Badiani, S.; Armstrong, F. A. The Value of Enzymes in Solar Fuels Research-Efficient Electrocatalysts through Evolution. *Chem. Soc. Rev.* **2019**, *48* (7), 2039−2052.
(24) Mazurenko, I.; Hitaishi, V. P.; Lojou, E. Recent Advances in Surface Chemistry of Electrodes to Promote Direct Enzymatic Bioelectrocatalysis. *Curr. Opin. Electrochem.* **2020**, *19*, 113−121.
(25) Smutok, O.; Kavetskyy, T.; Katz, E. Recent Trends in Enzyme Engineering Aiming to Improve Bioelectrocatalysis Proceeding with Direct Electron Transfer. *Curr. Opin. Electrochem.* **2022**, *31*, 100856.
(26) Heller, A. Electrical Wiring of Redox Enzymes. *Acc. Chem. Res.* **1990**, *23* (5), 128−134.
(27) Gao, W.; Emaminejad, S.; Nyein, H. Y. Y.; Challa, S.; Chen, K.; Peck, A.; Fahad, H. M.; Ota, H.; Shiraki, H.; Kiriya, D.; Lien, D. H.; Brooks, G. A.; Davis, R. W.; Javey, A. Fully Integrated Wearable Sensor Arrays for Multiplexed in situ Perspiration Analysis. *Nature* **2016**, *529* (7587), 509−514.
(28) Bruen, D.; Delaney, C.; Florea, L.; Diamond, D. Glucose Sensing for Diabetes Monitoring: Recent Developments. *Sensors (Switzerland)* **2017**, *17* (8), 1866.
(29) Teymourian, H.; Barfidokht, A.; Wang, J. Electrochemical Glucose Sensors in Diabetes Management: An Updated Review (2010−2020). *Chem. Soc. Rev.* **2020**, *49* (21), 7671−7709.
(30) Datta, S.; Mori, Y.; Takagi, K.; Kawaguchi, K.; Chen, Z. W.; Okajima, T.; Kuroda, S.; Ikeda, T.; Kano, K.; Tanizawa, K.; Mathews, F. S. Structure of a Quinohemoprotein Amine Dehydrogenase with an Uncommon Redox Cofactor and Highly Unusual Crosslinking. *Proc. Natl. Acad. Sci. U.S.A.* **2001**, *98* (25), 14268−14273.
(31) Liu, J.; Chakraborty, S.; Hosseinzadeh, P.; Yu, Y.; Tian, S.; Petrik, I.; Bhagi, A.; Lu, Y. Metalloproteins Containing Cytochrome, Iron-Sulfur, or Copper Redox Centers. *Chem. Rev.* **2014**, *114* (8), 4366−4369.
(32) Takeda, K.; Nakamura, N. Direct Electron Transfer Process of Pyrroloquinoline Quinone-Dependent and Flavin Adenine Dinucleotide-Dependent Dehydrogenases: Fundamentals and Applications. *Curr. Opin. Electrochem.* **2021**, *29*, 100747.
(33) Ikeda, T.; Kobayashi, D.; Matsushita, F.; Sagara, T.; Niki, K. Bioelectrocatalysis at Electrodes Coated with Alcohol Dehydrogenase, a Quinohemoprotein with Heme c Serving as a Built-in Mediator. *J. Electroanal. Chem.* **1993**, *361* (1−2), 221−228.
(34) Adachi, T.; Kitazumi, Y.; Shirai, O.; Kano, K. Direct Electron Transfer-Type Bioelectrocatalysis by Membrane-Bound Aldehyde Dehydrogenase from Gluconobacter Oxydans and Cyanide Effects on its Bioelectrocatalytic Properties. *Electrochem. Commun.* **2021**, *123*, 106911.
(35) Treu, B. L.; Arechederra, R.; Minteer, S. D. Bioelectrocatalysis of Ethanol via PQQ-Dependent Dehydrogenases Utilizing Carbon Nanomaterial Supports. *J. Nanosci. Nanotechnol.* **2009**, *9* (4), 2374−2380.
(36) Kakehi, N.; Yamazaki, T.; Tsugawa, W.; Sode, K. A Novel Wireless Glucose Sensor Employing Direct Electron Transfer Principle Based Enzyme Fuel Cell. *Biosens. Bioelectron.* **2007**, *22* (9−10), 2250−2255.
(37) Ikeda, T.; Matsushita, F.; Senda, M. Amperometric Fructose Sensor Based on Direct Bioelectrocatalysis. *Biosens. Bioelectron.* **1991**, *6* (4), 299−304.
(38) Okuda-Shimazaki, J.; Yoshida, H.; Sode, K. FAD Dependent Glucose Dehydrogenases - Discovery and Engineering of Representative Glucose Sensing Enzymes -. *Bioelectrochemistry* **2020**, *132*, 107414.
(39) Adachi, T.; Kaida, Y.; Kitazumi, Y.; Shirai, O.; Kano, K. Bioelectrocatalytic Performance of D-Fructose Dehydrogenase. *Bioelectrochemistry* **2019**, *129*, 1−9.
(40) Yamaoka, H.; Ferri, S.; Sode, M. F. K. Essential Role of the Small Subunit of Thermostable Glucose Dehydrogenase from *Burkholderia cepacia*. *Biotechnol. Lett.* **2004**, *26* (22), 1757−1761.
(41) Yoshida, H.; Kojima, K.; Shiota, M.; Yoshimatsu, K.; Yamazaki, T.; Ferri, S.; Tsugawa, W.; Kamitori, S.; Sode, K. X-Ray Structure of the Direct Electron Transfer-Type FAD Glucose Dehydrogenase Catalytic Subunit Complexed with a Hitchhiker Protein. *Acta Crystallogr. Sect. D Struct. Biol.* **2019**, *75*, 841−851.
(42) Shiota, M.; Yamazaki, T.; Yoshimatsu, K.; Kojima, K.; Tsugawa, W.; Ferri, S.; Sode, K. An Fe-S Cluster in the Conserved Cys-Rich Region in the Catalytic Subunit of FAD-Dependent Dehydrogenase Complexes. *Bioelectrochemistry* **2016**, *112*, 178−183.

(43) Okuda-Shimazaki, J.; Yoshida, H.; Lee, I.; Kojima, K.; Suzuki, N.; Tsugawa, W.; Yamada, M.; Inaka, K.; Tanaka, H.; Sode, K. Microgravity environment grown crystal tructure information based engineering of direct electron transfer type glucose dehydrogenase. *Commun. Biol.* **2022**, *5*, 1334.
(44) Ameyama, M.; Shinagawa, E.; Matsushita, K.; Adachi, O. D-Fructose Dehydrogenase of *Gluconobacter Industrius*: Purification, Characterization, and Application to Enzymatic Microdetermination of D-Fructose. *J. Bacteriol.* **1981**, *145* (2), 814−823.
(45) Kawai, S.; Goda-Tsutsumi, M.; Yakushi, T.; Kano, K.; Matsushita, K. Heterologous Overexpression and Characterization of a Flavoprotein-Cytochrome c Complex Fructose Dehydrogenase of *Gluconobacter Japonicus* NBRC3260. *Appl. Environ. Microbiol.* **2013**, *79* (5), 1654−1660.
(46) Kawai, S.; Yakushi, T.; Matsushita, K.; Kitazumi, Y.; Shirai, O.; Kano, K. The Electron Transfer Pathway in Direct Electrochemical Communication of Fructose Dehydrogenase with Electrodes. *Electrochem. commun.* **2014**, *38*, 28−31.
(47) Suzuki, Y.; Sowa, K.; Kitazumi, Y.; Shirai, O. The Redox Potential Measurements for Heme Moieties in Variants of D-Fructose Dehydrogenase Based on Mediator-Assisted Potentiometric Titration. *Electrochemistry* **2021**, *89*, 337−339.
(48) Hibino, Y.; Kawai, S.; Kitazumi, Y.; Shirai, O.; Kano, K. Mutation of Heme *c* Axial Ligands in D-Fructose Dehydrogenase for Investigation of Electron Transfer Pathways and Reduction of Overpotential in Direct Electron Transfer-Type Bioelectrocatalysis. *Electrochem. commun.* **2016**, *67*, 43−46.
(49) Hibino, Y.; Kawai, S.; Kitazumi, Y.; Shirai, O.; Kano, K. Construction of a Protein-Engineered Variant of D-Fructose Dehydrogenase for Direct Electron Transfer-Type Bioelectrocatalysis. *Electrochem. commun.* **2017**, *77*, 112−115.
(50) Kaida, Y.; Hibino, Y.; Kitazumi, Y.; Shirai, O.; Kano, K. Ultimate Downsizing of D-Fructose Dehydrogenase for Improving the Performance of Direct Electron Transfer-Type Bioelectrocatalysis. *Electrochem. Commun.* **2019**, *98*, 101−105.
(51) Suzuki, Y.; Makino, F.; Miyata, T.; Tanaka, H.; Namba, K.; Kano, K.; Sowa, K.; Kitazumi, Y.; Shirai, O. Structural and Bioelectrochemical Elucidation of Direct Electron Transfer-Type Membrane-Bound Fructose Dehydrogenase. *ChemRxiv* **2022**, DOI: 10.26434/chemrxiv-2022-d7hl9.
(52) Farver, O.; Skov, L. K.; Young, S.; Bonander, N.; Karlsson, B.; Vanngard, T. G.; Pecht, I. Aromatic Residues May Enhance Intramolecular Electron Transfer in Azurin. *J. Am. Chem. Soc.* **1997**, *119* (23), 5453−5454.
(53) Shih, C.; Museth, A. K.; Abrahamsson, M.; Blanco-Rodriguez, A. M.; Di Bilio, A. J.; Sudhamsu, J.; Crane, B. R.; Ronayne, K. L.; Towrie, M.; Vlček, A.; Richards, J. H.; Winkler, J. R.; Gray, H. B. Tryptophan-Accelerated Electron Flow through Proteins. *Science (80-.).* **2008**, *320* (5884), 1760−1762.
(54) Takematsu, K.; Williamson, H.; Blanco-Rodríguez, A. M.; Sokolová, L.; Nikolovski, P.; Kaiser, J. T.; Towrie, M.; Clark, I. P.; Vlček, A.; Winkler, J. R.; Gray, H. B. Tryptophan-Accelerated Electron Flow across a Protein-Protein Interface. *J. Am. Chem. Soc.* **2013**, *135* (41), 15515−15525.
(55) Takematsu, K.; Williamson, H. R.; Nikolovski, P.; Kaiser, J. T.; Sheng, Y.; Pospíšil, P.; Towrie, M.; Heyda, J.; Hollas, D.; Záliš, S.; Gray, H. B.; Vlček, A.; Winkler, J. R. Two Tryptophans Are Better Than One in Accelerating Electron Flow through a Protein. *ACS Cent. Sci.* **2019**, *5* (1), 192−200.
(56) Sarhangi, S. M.; Matyushov, D. V. Theory of Protein Charge Transfer: Electron Transfer between Tryptophan Residue and Active Site of Azurin. *J. Phys. Chem. B* **2022**, *126* (49), 10360−10373.
(57) Olloqui-Sariego, J. L.; Zakharova, G. S.; Poloznikov, A. A.; Calvente, J. J.; Hushpulian, D. M.; Gorton, L.; Andreu, R. Influence of Tryptophan Mutation on the Direct Electron Transfer of Immobilized Tobacco Peroxidase. *Electrochim. Acta* **2020**, *351*, 136465.
(58) Sugimoto, Y.; Kawai, S.; Kitazumi, Y.; Shirai, O.; Kano, K. Function of C-Terminal Hydrophobic Region in Fructose Dehydrogenase. *Electrochim. Acta* **2015**, *176*, 976−981.
(59) Winkler, J. R.; Gray, H. B. Electron Flow through Metalloproteins. *Chem. Rev.* **2014**, *114* (7), 3369−3380.
(60) Page, C. C.; Moser, C. C.; Chen, X.; Dutton, P. L. Natural Engineering Principles of Electron Tunnelling in Biological Oxidation-Reduction. *Nature* **1999**, *402* (6757), 47−52.
(61) Matsushita, K.; Kobayashi, Y.; Mizuguchi, M.; Toyama, H.; Adachi, O.; Sakamoto, K.; Miyoshi, H. A Tightly Bound Quinone Functions in the Ubiquinone Reaction Sites of Quinoprotein Alcohol Dehydrogenase of an Acetic Acid Bacterium, *Gluconobacter Suboxydans*. *Biosci. Biotechnol. Biochem.* **2008**, *72* (10), 2723−2731.
(62) Yakushi, T.; Matsushita, K. Alcohol Dehydrogenase of Acetic Acid Bacteria: Structure, Mode of Action, and Applications in Biotechnology. *Appl. Microbiol. Biotechnol.* **2010**, *86* (5), 1257−1265.
(63) Adachi, T.; Miyata, T.; Makino, F.; Tanaka, H.; Namba, K.; Kano, K.; Sowa, K.; Kitazumi, Y.; Shirai, O. Experimental and Theoretical Insights into Bienzymatic Cascade for Mediatorless Bioelectrochemical Ethanol Oxidation with Alcohol and Aldehyde Dehydrogenases. *ACS. Catal.* **2023**, *13*, 7955−7965.
(64) Bollella, P.; Hibino, Y.; Kano, K.; Gorton, L.; Antiochia, R. The Influence of pH and Divalent/Monovalent Cations on the Internal Electron Transfer (IET), Enzymatic Activity, and Structure of Fructose Dehydrogenase. *Anal. Bioanal. Chem.* **2018**, *410* (14), 3253−3264.
(65) Jumper, J.; Evans, R.; Pritzel, A.; Green, T.; Figurnov, M.; Ronneberger, O.; Tunyasuvunakool, K.; Bates, R.; Žídek, A.; Potapenko, A.; Bridgland, A.; Meyer, C.; Kohl, S. A. A.; Ballard, A. J.; Cowie, A.; Romera-Paredes, B.; Nikolov, S.; Jain, R.; Adler, J.; Back, T.; Petersen, S.; Reiman, D.; Clancy, E.; Zielinski, M.; Steinegger, M.; Pacholska, M.; Berghammer, T.; Bodenstein, S.; Silver, D.; Vinyals, O.; Senior, A. W.; Kavukcuoglu, K.; Kohli, P.; Hassabis, D. Highly Accurate Protein Structure Prediction with AlphaFold. *Nature* **2021**, *596* (7873), 583−589.
(66) Marcus, R. A.; Sutin, N. Electron transfers in chemistry and biology. *Biochim. Biophys. Acta. Bioenerg.* **1985**, *811* (3), 265−322.
(67) Lowe, H.J.; Clark, W. M. Studies on Oxidation-Reduction. XXIV. Oxidation-Reduction Potentials of Flavin Adenine Dinucleotide. *J. Biol. Chem.* **1956**, *221* (2), 983−992.
(68) Moser, C. C.; Keske, J. M.; Warncke, K.; Farid, R. S.; Dutton, P. L. Nature of Biological Electron Transfer. *Nature* **1992**, *355* (6363), 796−802.
(69) Farver, O.; Skov, L. K.; Pascher, T.; Karlsson, B. G.; Nordling, M.; Lundberg, L. G.; Vaenngaard, T.; Pecht, I. Intramolecular Electron Transfer in Single-Site-Mutated Azurins. *Biochemistry* **1993**, *32* (28), 7317−7322.
(70) Beratan, D. N.; Onuchic, J. N.; Betts, J. N.; Bowler, B. E.; Gray, H. B. Electron-Tunneling Pathways in Ruthenated Proteins. *J. Am. Chem. Soc.* **1990**, *112* (22), 7915−7921.
(71) Dolinsky, T. J.; Nielsen, J. E.; McCammon, J. A.; Baker, N. A. PDB2PQR: An Automated Pipeline for the Setup of Poisson-Boltzmann Electrostatics Calculations. *Nucleic Acids Res.* **2004**, *32* (Web Server), W665−W667.
(72) Baker, N. A.; Sept, D.; Joseph, S.; Holst, M. J.; McCammon, J. A. Electrostatics of Nanosystems: Application to Microtubules and the Ribosome. *Proc. Natl. Acad. Sci. U. S. A.* **2001**, *98* (18), 10037−10041.
(73) Bollella, P.; Hibino, Y.; Kano, K.; Gorton, L.; Antiochia, R. Highly Sensitive Membraneless Fructose Biosensor Based on Fructose Dehydrogenase Immobilized onto Aryl Thiol Modified Highly Porous Gold Electrode: Characterization and Application in Food Samples. *Anal. Chem.* **2018**, *90* (20), 12131−12136.
(74) Bocanegra-Rodríguez, S.; Molins-Legua, C.; Campíns-Falcó, P.; Giroud, F.; Gross, A. J.; Cosnier, S. Monofunctional Pyrenes at Carbon Nanotube Electrodes for Direct Electron Transfer H_2O_2 Reduction with HRP and HRP-Bacterial Nanocellulose. *Biosens. Bioelectron.* **2021**, *187*, 113304.
(75) Blanford, C. F.; Heath, R. S.; Armstrong, F. A. A Stable Electrode for High-Potential, Electrocatalytic O_2 Reduction Based on Rational Attachment of a Blue Copper Oxidase to a Graphite Surface. *Chem. Commun.* **2007**, No. 17, 1710−1712.

(76) Meredith, M. T.; Minson, M.; Hickey, D.; Artyushkova, K.; Glatzhofer, D. T.; Minteer, S. D. Anthracene-Modified Multi-Walled Carbon Nanotubes as Direct Electron Transfer Scaffolds for Enzymatic Oxygen Reduction. *ACS Catal.* **2011**, *1* (12), 1683−1690.
(77) Bollella, P.; Hibino, Y.; Kano, K.; Gorton, L.; Antiochia, R. Enhanced Direct Electron Transfer of Fructose Dehydrogenase Rationally Immobilized on a 2-Aminoanthracene Diazonium Cation Grafted Single-Walled Carbon Nanotube Based Electrode. *ACS Catal.* **2018**, *8* (11), 10279−10289.
(78) Léger, C.; Jones, A. K.; Albracht, S. P. J.; Armstrong, F. A. Effect of a Dispersion of Interfacial Electron Transfer Rates on Steady State Catalytic Electron Transport in [NiFe]-Hydrogenase and Other Enzymes. *J. Phys. Chem. B* **2002**, *106* (50), 13058−13063.
(79) Sugimoto, Y.; Kitazumi, Y.; Shirai, O.; Kano, K. Effects of Mesoporous Structures on Direct Electron Transfer-Type Bioelectrocatalysis: Facts and Simulation on a Three-Dimensional Model of Random Orientation of Enzymes. *Electrochemistry* **2017**, *85* (2), 82−87.

https://doi.org/10.1021/acscatal.3c03769
ACS Catal. 2023, 13, 13828−13837